Design of Industrial Water-Based Polymerization Agitated Vessel by CFD Simulation

Heidari, Amir*+

Process Simulation and Modeling Laboratory (PSMlab.ir), Faculty of Chemical, Petroleum and Gas Engineering, Semnan University, Semnan, I.R. IRAN

Karim Nejadian, Samrand

Petro Tarh Mabna Co., Tehran, I.R. IRAN

ABSTRACT: *The agitated vessels are frequently used equipment in industries, especially in polymer processes. In the present work, the CFD simulation technique was used to study the effect of impeller shapes in the industrial scale water-based polymers agitated vessels to increase mixing efficiency. The VOF multiphase approach and RNG $k-\varepsilon$ turbulent model were used to study the hydrodynamic behavior of fluids in the vessel. The simulations were done in four designs, including designs A, B, C, and D. Designs A and B had three curved impellers with two $59°$ blades for each one and one straight impeller at the vessel bottom. Results showed that in designs A and B the gas phase entered the liquid (polymer) phase and caused foaming liquid. In design C, a geometrical modification was done by removing the top curved impeller, adding a blade for curved impellers, and reducing of curved blade angle from 59° to 26°. Results showed that wide rotational zones were achieved (about 75% of the illiquid phase), and the liquid foaming problem was solved in design C. The modification of the bottom impeller in design D showed that the rotational zones cover about 95% of the entire liquid phase, which is the best performance compared to other designs. Also, the performance of design D was evaluated at the viscosity values, including $7\ kg/m.s$, $4\ kg/m.s$ and $1kg/m.s$ and mixing quality was validated at these values.*

KEYWORDS: *CFD simulation; Mixing; Agitated vessel; RNG $k-\varepsilon$ model; Water-based polymer.*

INTRODUCTION

Today water-based polymers, due to their ease of production, low cost, desirable properties, and fewer environmental hazards, are widely used globally. As a result, increasing the production efficiency of water-based polymers is essential to respond to the global demand for such polymers. The mixing tanks have the most vital role in enhancing product quality during water-based polymer production. Designing high-efficiency mixing equipment in the chemical industry is one of the most important issues for engineers. Today, various mixing equipment has been designed by researchers. Agitated vessels are one of the most widely used types of mixing equipment. According to the volume and height of the vessel, fluid characteristics, desired mixing time, and the multiphase process conditions, the different

* *To whom correspondence should be addressed.*
+E-mail address: amirheidari@semnan.ac.ir
1021-9986/2022/12/4158-4169 12/$/6.02

numbers, and shapes of impellers have been introduced to increase the mixing quality. It should be noted that poor mixing in various chemical processes can cost industries up to several hundred million dollars per year [1].

One of the most important techniques for studying and designing agitated vessels is the Computational Fluid Dynamics (CFD) method. An important feature of the CFD method is studying the effect of various parameters such as the shape, number and position of the impellers on the mixing quality of agitated vessels. This section reviews some of the research on simulating CFD mixing tanks. One of the techniques used in the CFD simulation of mixing vessels is the "Black Box" method. In this method, the boundary conditions of the impeller are extracted based on laboratory data and applied to the plate that surrounds the impeller. References [2, 3] can be mentioned among the researches that used the black box method. In the Black Box method, the parameters applied in the boundary conditions include tangential velocity, angular velocity, kinematic energy of turbulent current (k) and turbulent energy dissipation rate (ε), which must be measured experimentally. Therefore, if the impeller shape, vessel geometry, and operating conditions change, the required parameters to apply the impeller boundary condition must be measured again. Although the Black Box method has been proposed as one of the first solutions in the field of CFD simulation of mixing vessels, it cannot be a reliable technique in the CFD simulations [4].

Another method used to simulate agitator tanks is the inner-outer (IO) approach. In this approach, the vessel is divided into two areas that overlap to some extent [5, 6]. In this method, the blade area is called the inner area, and the tank and baffles area, except for the impeller, is called the outer area. In the first step, CFD simulation is performed in the inner area. This area contains a reference surface for which the rotation speed is defined to apply the impeller effect to the flow field. In the second step, the initial calculation of the flow field in the inner region is used as the boundary conditions of the outer region. By calculating the results in the outer region based on the results of the inner region and the exchange of results between the inner and outer regions, calculations are performed until numerical stability in the solution is obtained [4].

One of the most widely used techniques for simulation agitator tanks is the Moving Reference Frame (MRF) method. In this method, the effect of the impeller is simulated by defining two rotating and fixed regions. The impeller region is a rotating frame that rotates at a velocity equal to the impeller, and the zone outside the rotating frame is considered a constant frame. There is no overlap between the inner and outer frames in the MRF method. In this method, based on the data of a rotating frame, the flow characteristics are calculated in the impeller zone. The results of the rotating frame are used as a boundary condition to calculate the flow characteristics in the constant frame, and reciprocally, the results of flow characteristics in the constant frame are used as boundary conditions for the rotating frame to finally reach the final answer and numerical convergence [4]. Some of the simulations performed by MRF method can be referred to references [7-10], whose results show a good agreement with laboratory data.

One of the crucial parameters that extremely affects the simulation accuracy in agitator's vessels is the choice of the turbulent flow model. In general, three categories have been used to predict the turbulent flow behavior in the mixing vessels, which are: 1) Reynolds Averaged Navier-Stokes equations (RANS) 2) Reynolds Stress Models [11-14] 3) Models based on Large Eddy Simulation (LES) [15-17] 4) Direct Numerical Simulation (DNS) [18, 19]. Among the mentioned methods, RANS models, especially standard $k-\varepsilon$ and $RNG\ k-\varepsilon$ models, due to have received more attention from researchers due to extensive validation and less computational time than other models. Among the researches based on the standard $k-\varepsilon$ model, the references [20-27] and the $RNG\ k-\varepsilon$ model [28-32] can be mentioned.

The main purpose of this study is to achieve the appropriate shape, number, and position of the impellers in the water-based resin industrial agitated vessel, through which the proper rotational behavior occurs in the whole vessel. To achieve this goal, the CFD technique has studied several different geometric designs of the impellers to obtain the best geometric structure of the impeller's blades and impellers' position in the agitated industrial vessel.

CFD MODEL

Continuity and momentum equation

The continuity and momentum equations for a single-phase system based on Reynolds averaging method is expressed as follows:

$$\frac{\partial(\rho)}{\partial t}+\frac{\partial}{\partial x_i}(\rho u_i)=0 \quad (1)$$

$$\frac{\partial(\rho u_i)}{\partial t}+\frac{\partial}{\partial x_j}\left(\rho u_i u_j\right)=-\frac{\partial P}{\partial x_i}+\frac{\partial}{\partial x_i}\left(\mu_{lam}\left(\frac{\partial u_i}{\partial x_j}+\frac{\partial u_j}{\partial x_i}-\frac{2}{3}\delta_{ij}\frac{\partial u_I}{\partial x_I}\right)\right)+\frac{\partial}{\partial x_j}\left(-\rho\overline{u_j' u_i'}\right)+\rho g \quad (2)$$

where u, u', ρ, P, μ_{lam}, g and $\overline{u_j' u_i'}$ are time-averaged velocity, velocity fluctuations, density, pressure, laminar viscosity, gravity acceleration and Reynolds stress term, respectively. Reynolds stress is expressed as follows based on the Boussinesq approach [33]:

$$-\rho\overline{u_j' u_i'}=\mu_t\left(\frac{\partial u_i}{\partial x_j}+\frac{\partial u_j}{\partial x_i}\right)-\frac{2}{3}\left(\rho k+\mu_t\frac{\partial u_I}{\partial x_I}\right)\delta_{ij} \quad (3)$$

where μ_t and k are the viscosity and kinetic energy of the turbulent flow and can be calculated by turbulent flow equations such as $RNG\ k-\varepsilon$.

Turbulent model equations

In this research, the $RNG\ k-\varepsilon$ equation was used to simulate the turbulent flow behavior. Among the $k-\varepsilon$ models, the $RNG\ k-\varepsilon$ model has a better ability to predict turbulent flow regime within agitated vessels due to its modifications to account for rotational flow effects [34]. The conservation equations of eddies kinetic energy (k) and the energy dissipation (ε) are as follows:

$$\frac{\partial(\rho k)}{\partial t}+\frac{\partial}{\partial x_i}(\rho k u_i)=\frac{\partial}{\partial x_j}\left(\alpha_k(\mu_{lam}+\mu_t)\frac{\partial k}{\partial x_j}\right)+G_k-\rho\varepsilon \quad (4)$$

$$\frac{\partial(\rho\varepsilon)}{\partial t}+\frac{\partial}{\partial x_i}(\rho\varepsilon u_i)=\frac{\partial}{\partial x_j}\left(\alpha_\varepsilon(\mu_{lam}+\mu_t)\frac{\partial\varepsilon}{\partial x_j}\right)+C_{1\varepsilon}\frac{\varepsilon}{k}G_k-C_{2\varepsilon}^{*}\rho\frac{\varepsilon^2}{k} \quad (5)$$

Where $C_{1\varepsilon}$ is a fixed constant with values of 1.42 [34]. Also α_k and α_ε are proportional to the inverse of Prandtl number for k and ε. In Eqs (4) and (5) the μ_t is the turbulent flow viscosity, which is calculated by:

$$\mu_t=\rho C_\mu\frac{k^2}{\varepsilon} \quad (6)$$

Where C_μ is a constant with the value of 0.0845. The parameter $C_{2\varepsilon}^{*}$ in Eq. (5) is also calculated based on the following relations:

$$C_{2\varepsilon}^{*}=C_{2\varepsilon}+\frac{C_\mu\eta^3(1-\eta/\eta_0)}{1+\beta\eta^3} \quad (7)$$

$$\eta=\sqrt{2S_{ij}S_{ij}}\frac{k}{\varepsilon} \quad (8)$$

Where $C_{2\varepsilon}$, η_0 and β are equal to 1.68, 4.38 and 0.012, respectively.

Multiphase flow model

To simulate the behavior of liquid and gas fluid at the interface, the Volume of Fluid (VOF) multiphase model was used. In the VOF model, the conservation of the volume fraction of phases in each computational cell, when there is no interphase mass transfer, is calculated based on the following equation:

$$\frac{\partial}{\partial t}\left(\alpha_q\rho_q\right)+\nabla.\left(\alpha_q\rho_q u\right)=0 \quad (7)$$

Where α_q is the volume fraction of phase q. Also, the volume fraction for the last phase is calculated by the following equation:

$$\sum_{q=1}^{N}\alpha_q=1 \quad (8)$$

It should be noted that the following mixing law is used to calculate the density in the equations of Eqs (1-6):

$$\rho=\sum_{q=1}^{N}\alpha_q\rho_q \quad (9)$$

Also, the laminar flow viscosity in Eqs (2, 4) is calculated by the following equation:

$$\mu_{lam}=\sum_{q=1}^{N}\frac{\alpha_q\rho_q\mu_{lam_q}}{\alpha_q\rho_q} \quad (10)$$

Boundary conditions

The wall boundary conditions are the main boundary condition for the vessel walls in the current contribution. Due to batch operation of the process, inlet and outlet boundary conditions were not defined in the CFD model.

Numerical method and mixing technique

In this work, the finite volume method was used to solve the governing equations numerically. The SIMPLE (Semi-Implicit Method for Pressure Linked Equations) algorithm was used to solve the pressure-velocity field. Furthermore, the QUICK (Quadratic Upwind Interpolation for Convective Kinematics) discretization scheme was used to discretize the continuity, momentum, and turbulence equations. The MRF approach was used to simulate the effect of the impeller rotation on the hydrodynamic behavior of the vessel. In addition, the standard wall function model was used to model the flow field near the wall. The simulations

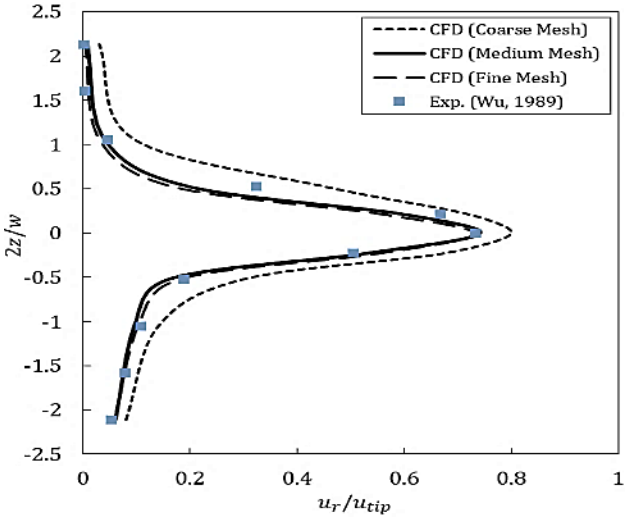

Fig. 1: Mesh independency and the validation of the CFD model at small scale

were carried out on a workstation with 24 GB RAM and 24 core Intel® Xeon® Processor.

RESULTS AND DISCUSSION

Validation and mesh independency

In order to validate the models and numerical solution procedure, the laboratory data presented by Wu and Patterson [35] were used for CFD results verification. Also, the geometry details can be found in reference [35]. The mesh independency for experimental work was evaluated at three different meshes, including coarse (cells number: 6.2×10^5), medium (cells number: 1.1×10^6) and fine (cells number: 1.9×10^6). Fig. 1 shows the CFD simulation results and laboratory data of the radial velocity distribution at 200 rpm at $r = 5\ cm$ at different distances from the top and bottom of the impeller. It can be seen that in the coarse mesh there is a large difference in the velocity distribution prediction compared to medium and fine meshes. On the other hand, the results of medium and fine mesh are very close to each other. The average relative error rate of CFD results and laboratory data for the medium mesh size was evaluated 4%, which showed a good agreement between CFD and laboratory data. According to the results, the capability of the models and numerical methods can also be ensured in the large-scale mixing tank simulation.

The mesh independency of large scale vessel was performed by evaluating the middle impeller power number at four different mesh sizes. The simulation results of studied mesh sizes are shown in Table 1. According to Table 1, mesh 3 (Mesh-LS-3) was chosen for all simulations due to being less computationally demanding.

Table 1: Mesh independency and the validation of the CFD model at large scale

Mesh type	Cells number	Power number
Mesh-LS-1	3458750	0.31
Mesh-LS-2	4825674	0.33
Mesh-LS-3	5935683	0.36
Mesh-LS-4	7021553	0.36

Design A

Geometric specifications of design A

In this research, four different geometries, including designs *A*, *B*, *C* and *D* of the industrial agitated vessel, were proposed to study the effect of impellers geometric details on the mixing quality. Fig. 2 depicts the vessel dimensions and impellers (curved and straight impellers) configuration and Fig. 3 depicts more details for the curved blades of design *A*. As shown in Fig. 2, the tank has a straight impeller with an angled bottom edge for the blades and the other three impellers contain two curved blades that their width reduces from the center to the impeller tip. The mixing process is performed based on the available industrial information for 1000 *kg* water-based polymer with the viscosity of 7 $kg/m.s$ and impeller speed of 60 *rpm*.

Hydrodynamic behavior of design A

Fig. 4-A shows the velocity vectors and contour of the volume fraction of the liquid phase on the cross section $y = 0$. Due to the formation of multiple rotational areas (white lines) as well as the effect of the upper impeller on the formation of the vortex zone on the liquid phase surface, a uniform distribution of flow was not observed in the vessel. In this study, the main purpose of the work was to create a uniform rotational flow in the tank to increase the quality of polymer mixing. Also, according to liquid phase properties, the liquid had a relatively high viscosity, and it was expected that small vortex zone forms at the gas-liquid interface, but according to the simulation results, it was seen that the upper impeller has a great effect on the size of vortex zone at the liquid interface. The formation of this vortex zone causes the entrance of the gas phase to the liquid phase (black circles in the figure), resulting in fluid foaming and a reduction in mixing and product

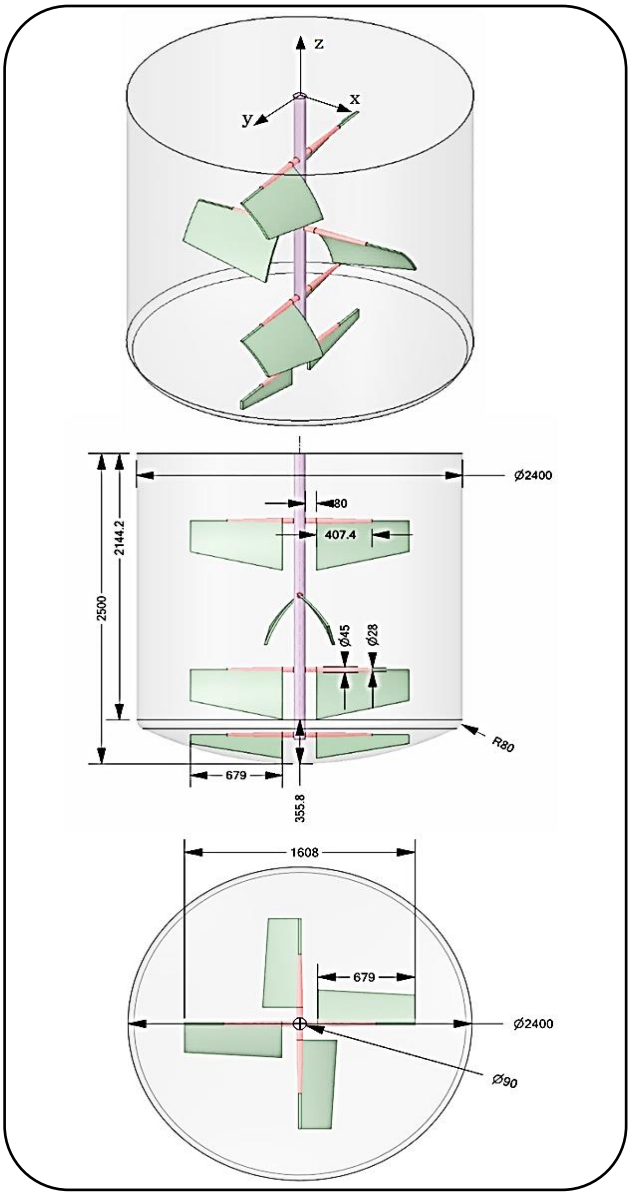

Fig. 2: Geometric details of design A (dimensions in mm)

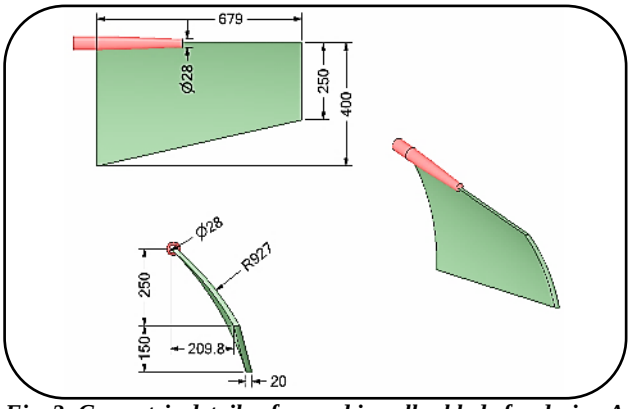

Fig. 3: Geometric details of curved impeller blade for design A (dimensions in mm)

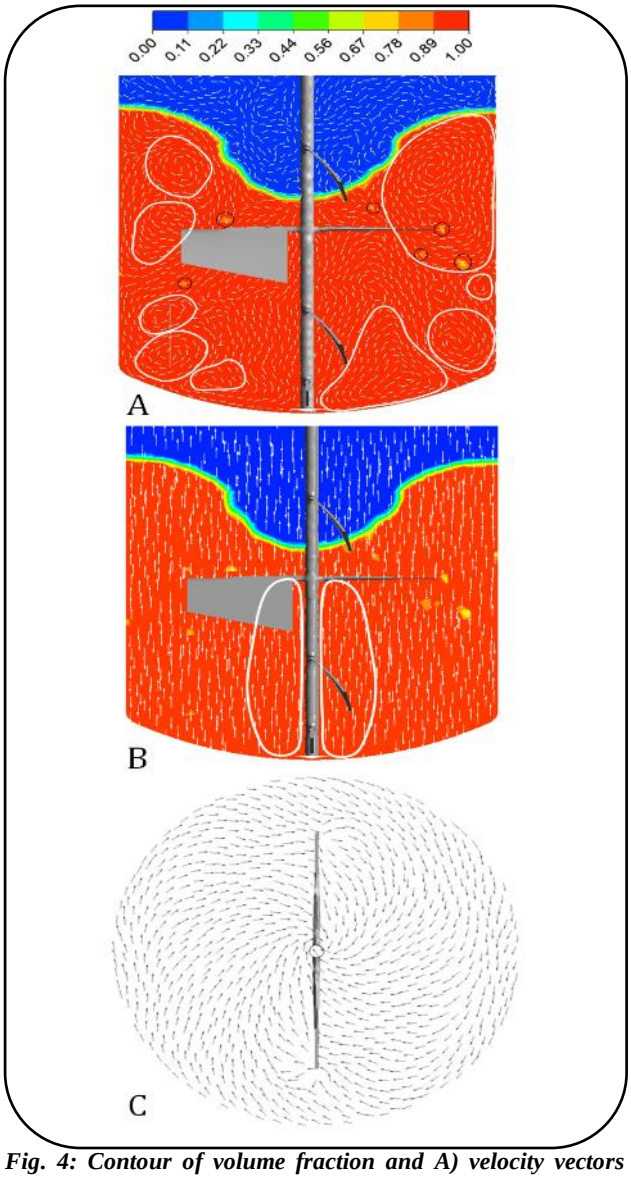

Fig. 4: Contour of volume fraction and A) velocity vectors (constant length) B) Axial (Z direction) velocity vectors (constant length) in section $y = 0$ B) Velocity vectors in the vessel bottom of design A

quality. So, before modifying the geometric structure and position of the impellers in design B, the effect of the baffle on the formation of the vortex zone on the gas-liquid interface is investigated in the next section. Another important point to consider about the hydrodynamic behavior of the vessel was to achieve a downward flow field along the vessel shaft. Based on the pattern of Axial (*Z* direction) velocity vectors in Fig. 4-B, it was observed that the dominant flow behavior is upward in the adjacent of the shaft, which showed adverse results for the hydrodynamic design goal of this study.

Fig. 4-C depicts velocity vectors of design *A* on the bottom of the vessel. The main function of the tank bottom impeller is the prevention of polymer deposition on the vessel bottom. For this purpose, the conduction of fluid in a radial direction from the center to the vessel sidewall can avoid polymer deposition. As Fig. 4-C shows the velocity vectors direction is from the tank sidewall to the tank axis, which is a reverse and inappropriate direction. Also, velocity vectors in Fig. 4 showed that the location of the bottom impeller suction is below the impeller and near the vessel shaft that in the optimal design the impeller suction should be at the top of the bottom impeller.

According to the distribution of velocity vectors of Fig. 4, it seems that the inappropriate results in hydrodynamics behavior of design *A* can be corrected by modifying the shape and location of the impellers. But, before making general corrections in the impeller configuration of design *A*, the impact of the baffle on the hydrodynamics behavior is examined in design *B*.

Design B

Geometric specifications of design B

Fig. 5 shows the dimensions and geometry of design *B* mixing vessel. The vessel geometric characteristics and fluid properties of design *B* were similar to design *A* except that two baffles were added to the vessel. The baffles had a gap with 50 mm distance from the sidewall to avoid poor mixing in the backside of the baffles. The purpose of adding baffles was to investigate their effect on the vortex zone created by the top impeller at the gas-liquid interface.

Hydrodynamic behavior of design B

Fig. 6-A depicts the velocity vectors and contour of the volume fraction of the liquid phase on the cross section $y = 0$ of design *B*. According to the figure, the vortex zone created on the gas-liquid interface in design B had found to be a small size compared to design *A*. But, in design *B*, similar to design *A*, the formation of this vortex zone caused to enter gas phase bubbles in the liquid phase (black circles). As shown in Fig. 6-A, several multiple rotational areas (white lines) were still observed in the liquid phase. In addition, the flow pattern around the vessel shaft was upward, which is an inappropriate flow pattern. According to the hydrodynamics results of designs *A* and *B* the top impeller has an inappropriate effect on the mixing quality and can be removed in the next designs.

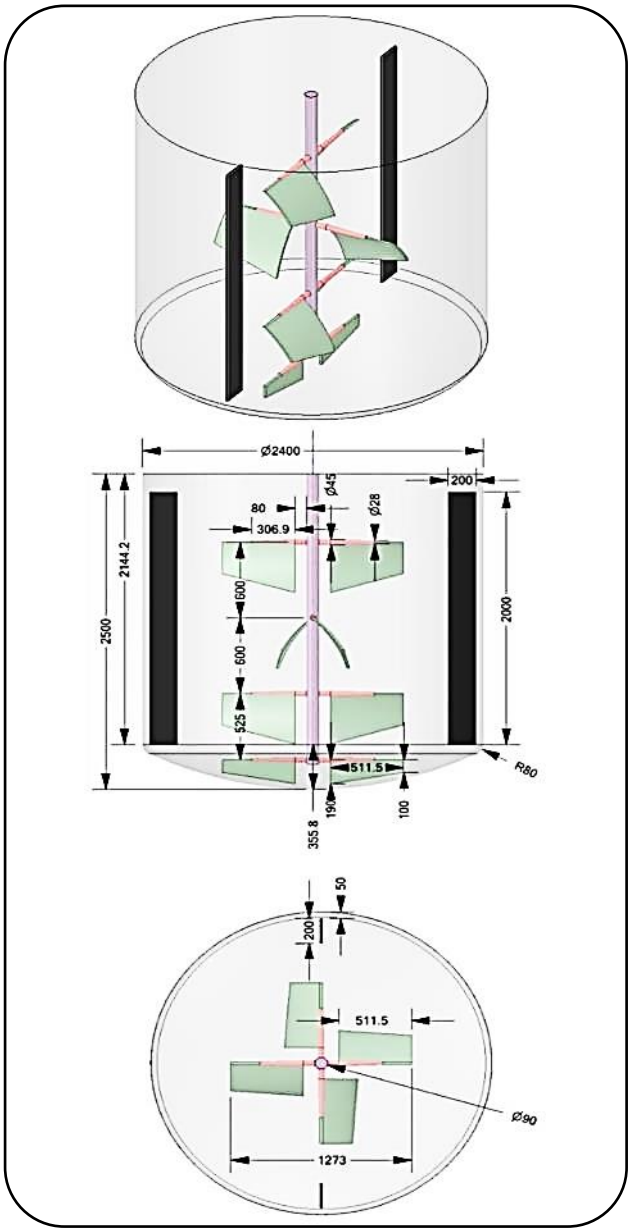

Fig. 5: Geometric details of design B (dimensions in mm)

Fig. 6-B depicts the velocity vectors at the bottom of the design *B* vessel. The results showed that the baffles could not significantly affect the flow pattern at the bottom of the vessel, and like design *A*, the direction of flow in the bottom of the tank is still towards the center of the vessel. Due to the fact that the desired hydrodynamic results were not achieved in designs *A* and *B*, therefore the flow pattern in the vessel was modified with the help of characteristic modifications of impellers angle and the number of blades. These modifications and their results are discussed in designs *C* and *D* in the next sections.

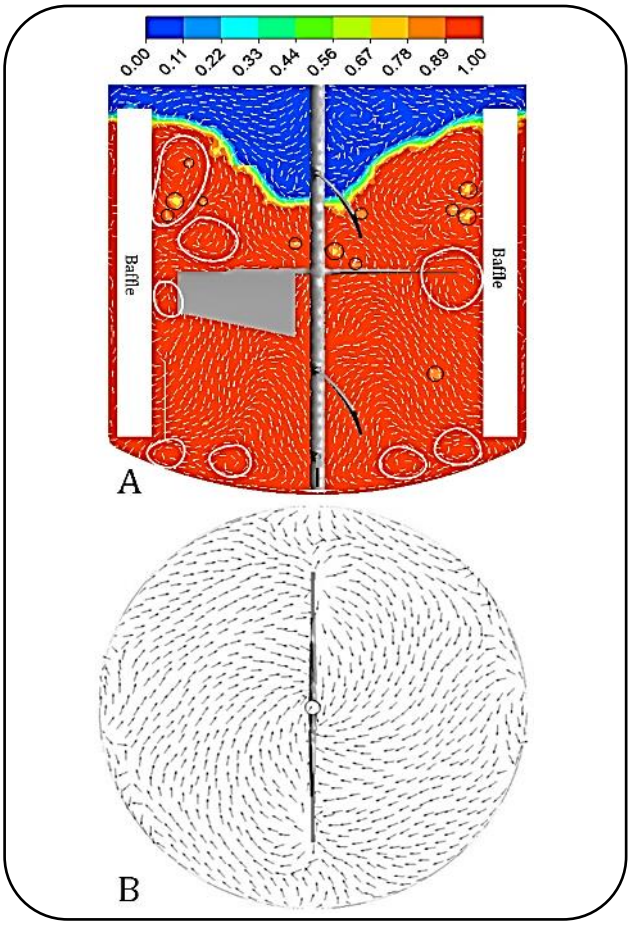

Fig. 6: A) Contour of volume fraction and velocity vectors (constant length) of liquid phase in section $y = 0$ and B) Velocity vectors in the vessel bottom of design B

Design C

Geometric specifications of design C

The hydrodynamic performance of the design *C* was evaluated by some modifications in designs *A* and *B*. These modifications were a) removing the top impeller b) reducing the angle of the curved blades from $59°$ of to $26°$ c) using a straight impeller with rectangular blade for bottom impeller and d) adding one more blade to the curved impeller (impeller with three blades). Figs. 7 and 8 show the vessel geometrical characteristic of design *C* and curved blade specification, respectively. It should be noted that the fluid properties and operating conditions of design *C* were similar to the presented conditions in design *A*.

Hydrodynamic behavior of design C

The velocity vectors and contour of the liquid phase volume fraction of design *C* are plotted on the cross section $y = 0$ in Fig. 9-A. According to the figure, the large

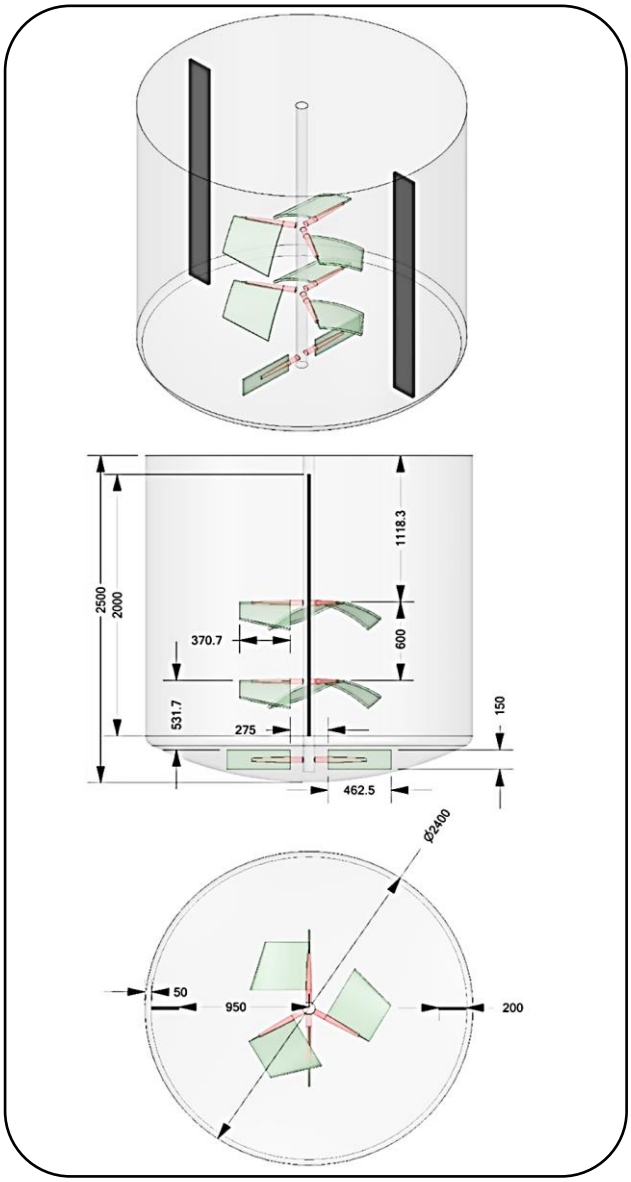

Fig. 7: Geometric details of design C (dimensions in mm)

rotational areas were formed around the curved impellers in the vessel (white lines). Also, it was inferred from Fig. 9-A that removal of the top impeller in designs *A* and *B* eliminated vortex zone formation in the gas-liquid interface and entrance of gas phase bubbles to the liquid phase. In addition, reducing the blade angle from $59°$ to $26°$ and increasing the number of impeller blades from two to three caused a downward flow current near the shaft and an upward current around the vessel sidewall. Achieving this type of rotational flow in the vessel was an important step in water-based polymer agitator vessels to reduce the possibility of foaming formation in the liquid phase and increase the wall-fluid heat exchange rate.

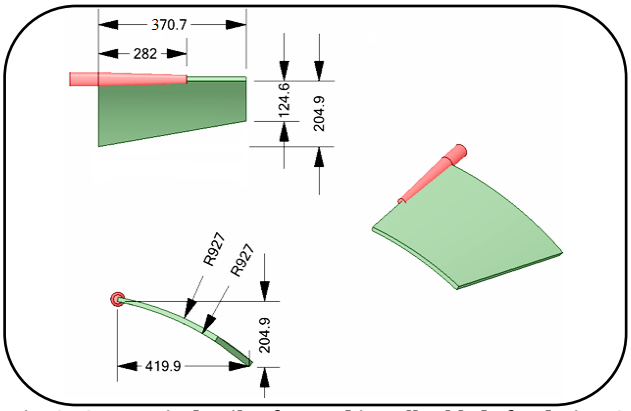

Fig. 8: Geometric details of curved impeller blade for design C (dimensions in mm).

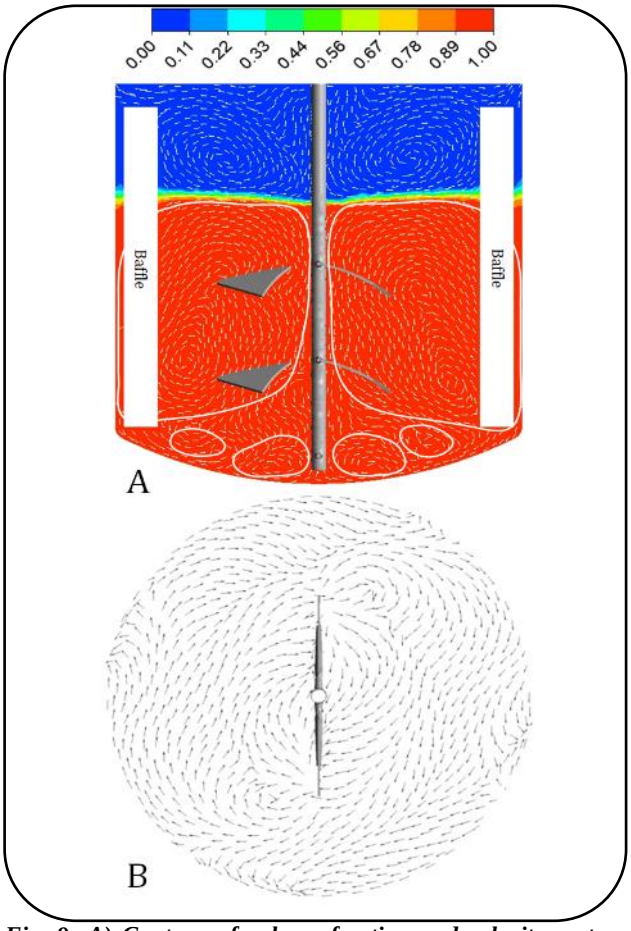

Fig. 9: A) Contour of volume fraction and velocity vectors (constant length) of the liquid phase in section $y = 0$ and B) Velocity vectors in the vessel bottom of design C.

Fig. 9-B depicts the velocity vectors of design *C* on the vessel bottom wall. According to the figure, the bottom impeller with rectangular blades did not conduct the flow of the vessel to the vessel sidewall and the flow pattern tended to move toward the center of the vessel. So, the bottom impeller needs geometric correction which is discussed in design *D*.

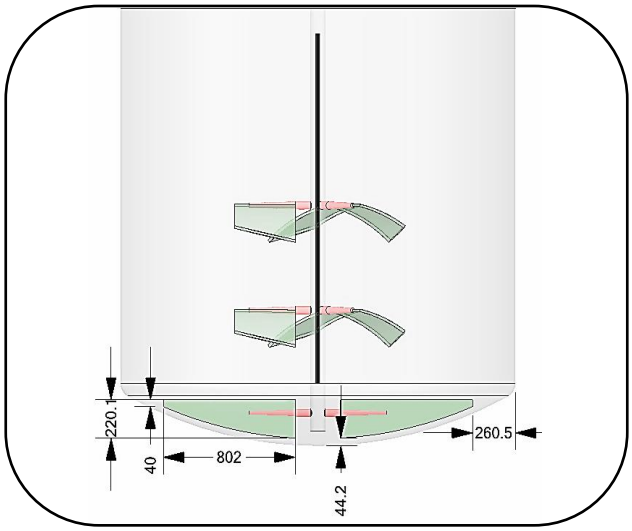

Fig. 10: Geometric dimension of the bottom impeller of design D

Design D

Geometric specifications of design D

To modify the hydrodynamic behavior of the fluid in the vessel bottom of design *C*, the geometric shape of the down impeller was modified in design *D*. All other geometric features of design *D* were similar to design *C*. Fig. 10 shows the geometric characteristics of the bottom impeller of design *D*. The main purposes of modification of the vessel down impeller were to improve the rotational area in the vessel and correction of the flow pattern at vessel bottom from center to sidewall by reduction of impeller and vessel bottom clearance and increase in length of the blades.

Hydrodynamic behavior of design D

Fig. 11-A depicts the velocity vectors and volume fraction contour of the liquid phase in the section $y = 0$ of design *D*. The velocity vector pattern showed a significant effect on the improvement of the rotational flow pattern of design *D* in comparison to design C (Fig. 9-A) so that, the rotational flow circulates in the entire vessel (white lines in Fig. 11-A). Fig. 11-B shows the effect of the lower impeller on the velocity vectors of the vessel bottom. Based on the figure, it can be concluded that the modified down impeller conducts the flow of the vessel bottom from the center to the sidewall. This flow pattern prevents the accumulation of high viscosity polymer

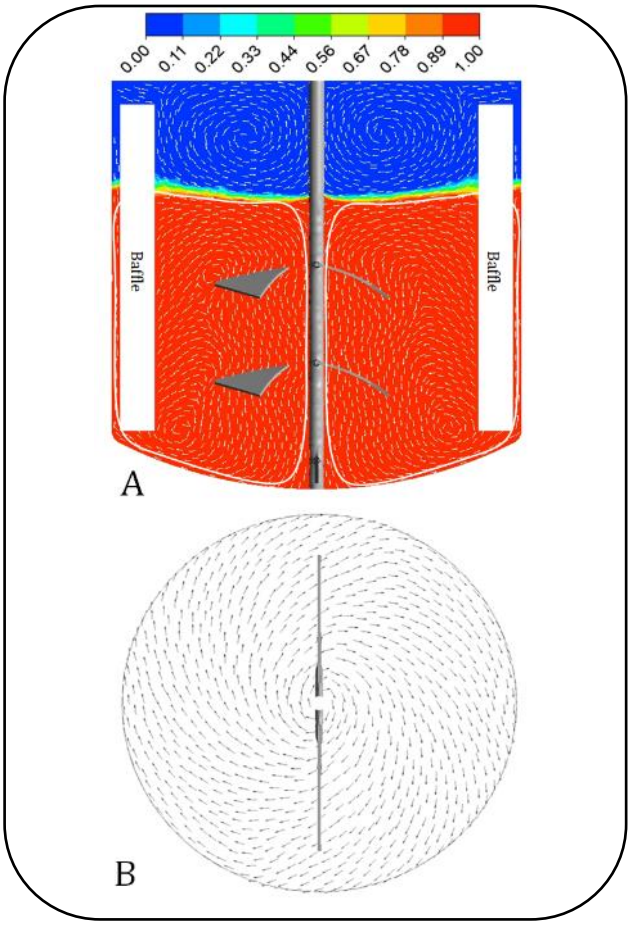

Fig. 11: A) Contour of volume fraction and velocity vectors (constant length) of the liquid phase in section $y = 0$ B) Velocity vectors in the vessel bottom of design D

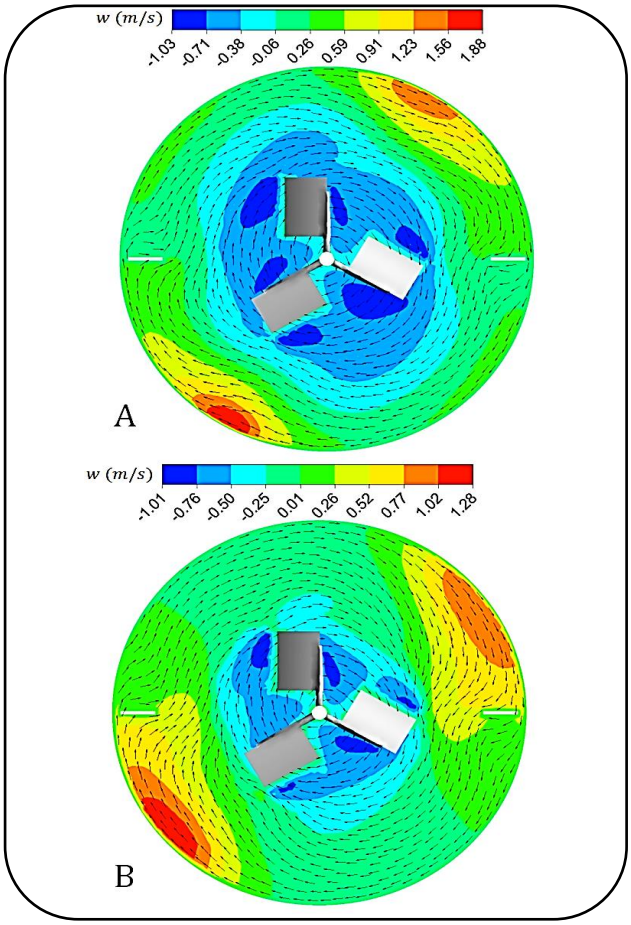

Fig. 12: Velocity vectors (constant length) and axial velocity contours (w) in A) the middle curved impeller at $z = 0.7\ m$ and B) the top curved impeller at $z = 1.3\ m$ of design D

phases in the tank bottom and the formation of polymer deposits in the vessel bottom.

Fig. 12 shows the velocity vectors and axial velocity (w) around the curved impellers of the design *D* at sections $z = 0.7\ m$ and $= 1.3\ m$. Due to the physical properties of the liquid phase and the operational condition, there was a uniform rotational flow around the impellers. In addition, according to the contour of axial flow, it could be concluded that the flow direction is downward around the vessel shaft and upward direction near the vessel sidewall.

Effect of fluid viscosity on the vessel hydrodynamic behavior

During the water-based polymer processing, the viscosity of the fluid changes during the process. In this section, the effect of viscosity was investigated on the mixing quality at three different values including 7 kg / m.s, 4 kg / m.s and 1 kg / m.s of design *D* vessel. Fig. 13 shows the velocity vectors in different viscosity values of design *D* at $y = 0$ section. Results showed that a complete rotational flow occurs in the vessel at all considered viscosities. Therefore, since the polymer viscosity changes during the process, the evaluated flow behavior in the vessel confirms the proper performance of design *D* at the formation of the overall rotational area at different viscosities.

CONCLUSIONS

In this contribution, an industrial agitated vessel of the water-based polymer was studied by the CFD technique. The hydrodynamic behavior of the fluid in the vessel was evaluated with VOF multiphase approach and *RNG* $k - \varepsilon$ turbulence model. The numerical methods and solution models were validated with reported experimental data by *Wu* and *Patterson* [35]. The results showed good agreement between CFD and reported experimental data [35].

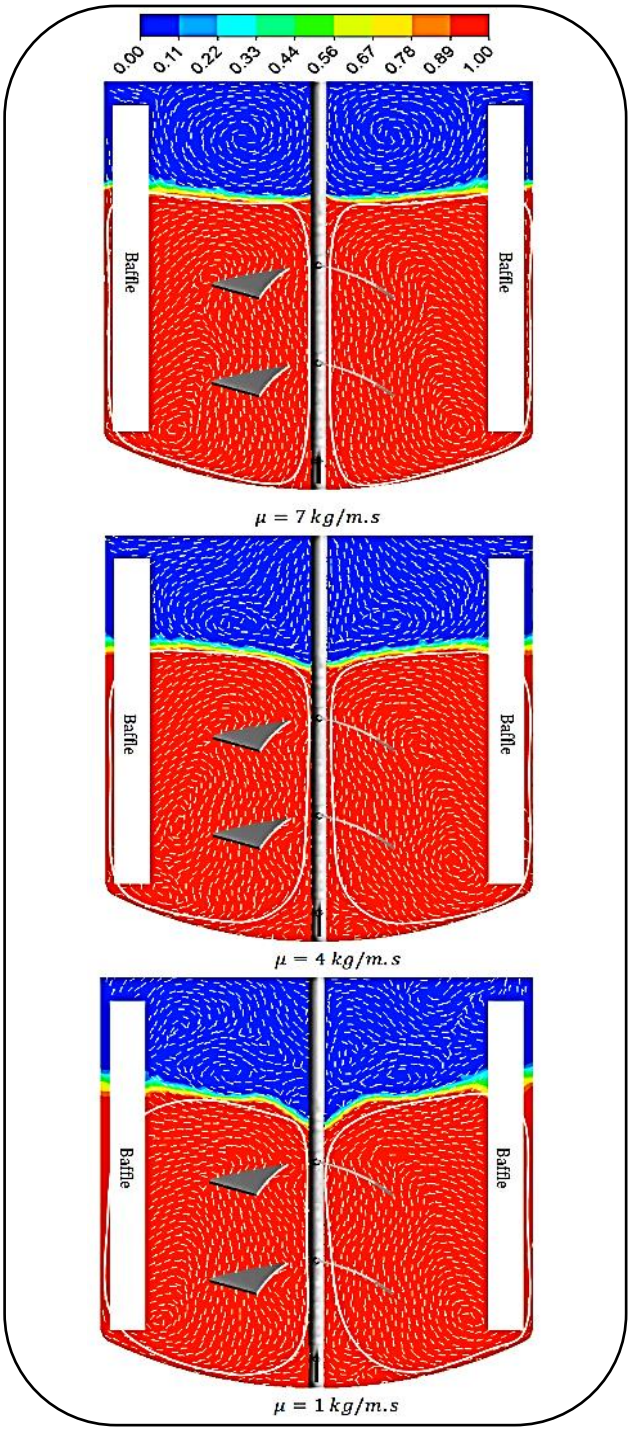

Fig. 13: Contour of volume fraction and velocity vectors (constant length) of the liquid phase in section $y = 0$ at different viscosities

The modification of the agitated vessel was done during the change in impellers and blades shapes and numbers at four designs, including design *A*, *B*, *C* and *D*. Hydrodynamics results showed the formation of a vortex area at the gas-liquid interface and foaming problems in designs *A* and *B* due to low distance of top impeller with the gas-liquid interface. Although using baffles in design *B* reduced the size of the vortex zone, but the foaming problem did not solve by adding baffles. In design *C*, the foaming problem was solved by removing the vessel top impeller. Also, adding one blade to the curved impellers and changing the blade angle from 59° to 26° formed a rotational zone from the top of the bottom impeller up to the gas-liquid interface, which caused the increase in mixing quality. In design *D*, an inappropriate flow pattern at the vessel bottom of design *C* was solved by an increase in length of the straight bottom impeller and a decrease in distance between the down edge of blades with the vessel bottom. Design *D* showed a global and perfect rotational zone from top to bottom of the vessel with the down flow at the vessel center and up-flow near the sidewall. Finally, by examining the three different liquid viscosity, including 7 kg/m.s, 4 kg/m.s and 1 kg/m.s it was shown that design *D* provides a global rotational zone at different viscosities which satisfies the mixing criteria in the polymerization agitated vessel.

Based on the current study investigations, future work could include further improvements in the impeller shape, number of impellers on the shaft, position of the impeller in the vessel, and combination of different impeller shapes on the mixing quality.

Acknowledgment

The authors wish to acknowledge the financial support provided by the Petro Tarh Mabna Company (Grant No. 9801-01).

Nomenclature

Constant numbers, dimensionless	$C_{1\varepsilon}, C_{2\varepsilon}$
Gravity, m / s^2	g
Turbulent kinematic energy production, $kg/m.s^3$	G_k
Turbulent kinetic energy, m^2/s^2	k
Pressure, $kg/m.s^2$	P
The rate of deformation, $1/s$	S_{ij}
Time, s	t
Velocity, m/s	u
Velocity fluctuation, m/s	u'
Impeller blade width, m	w
Direction, m	x
Axial coordinate	z

Volume fraction, dimensionless	α
Inverse of Prandtl number for k and ε	α_k
Inverse of Prandtl number for ε	α_ε
Constant, dimensionless	β
Energy dissipation rate, m^2/s^3	ε
Constant, dimensionless	η_0
Viscosity, $kg/m.s$	μ
Density, kg/m^3	ρ
Laminar	lam
q^{th} phase, q = G or L	q
Turbulence	t

Received: Jan. 2, 2022 ; Accepted: May. 16, 2022

REFERENCES

[1] Paul E.L., Kresta S.M., Atiemo-Obeng V.A., "Handbook of Industrial Mixing: Science and Practice", Wiley-Interscience, Hoboken, N.J. England, (2004).

[2] Kresta S.M., Wood P.E., Prediction of the Three-Dimensional Turbulent Flow in Stirred Tanks, *AIChE Journal*, **37(3):** 448-460 (1991).

[3] Ranade V.V., Joshi J.B., Flow Generated by a Disc Turbine. Part I. Mathematical Modelling and Comparison with Experimental Data, *Chemical Engineering Research and Design*, **68(1):** 34-50 (1990).

[4] Joshi J.B., Nere N.K., Rane C.V., Murthy B.N., Mathpati C.S., Patwardhan A.W., Ranade V.V., CFD Simulation of Stirred Tanks: Comparison of Turbulence Models. Part I: Radial Flow Impellers, *Canadian Journal of Chemical Engineering*, **89(1):** 23-82 (2011).

[5] Brucato A., Ciofalo M., Grisafi F., Micale G., Numerical Prediction of Flow Fields in Baffled Stirred Vessels: A Comparison of Alternative Modelling Approaches, *Chemical Engineering Science*, **53(21):** 3653-3684 (1998).

[6] Daskopoulos P., Harris C.K., "Three-Dimensional CFD Simulations of Turbulent Flow in Baffled Stirred Tanks: an Assessment of The Current Position", Institution of Chemical Engineers Symposium Series, Rugby, UK, (1996).

[7] Wodołażski A., Cfd-Population Balance Modelling of Catalyst Particles in Solid-Liquid Rushton Turbine-Agitated Tank Reactor in Scale-up Study, *Powder Technology*, **313:** 312-322 (2017).

[8] Kamla Y., Bouzit M., Hadjeb A., Arab I.M., Beloudane M., Cfd Study of the Effect of Baffles on the Energy Consumption and the Flow Structure in a Vessel Stirred by a Rushton Turbine, *Mechanika*, **22(3):** 190-197 (2016).

[9] Azargoshasb H., Mousavi S.M., Jamialahmadi O., Shojaosadati S.A., Mousavi S.B., Experiments and a Three-Phase Computational Fluid Dynamics (CFD) Simulation Coupled with Population Balance Equations of a Stirred Tank Bioreactor for High Cell Density Cultivation, *Canadian Journal of Chemical Engineering*, **94(1):** 20-32 (2016).

[10] Liang Y., Gao D., Bai L., Numerical Simulation of the Laminar Flow Field and Mixing Time in Stirred Tank with Double Layer Impeller, *Jixie Gongcheng Xuebao/Journal of Mechanical Engineering*, **51(16):** 185-195 (2015).

[11] Aghbolaghy M., Karimi A., Simulation and Optimization of Enzymatic Hydrogen Peroxide Production in a Continuous Stirred Tank Reactor Using Cfd–Rsm Combined Method, *Journal of the Taiwan Institute of Chemical Engineers*, **45(1):** 101-107 (2014).

[12] Vlček P., Skočilas J., Jirout T., Cfd Simulation of a Stirred Dished Bottom Vessel, *Acta Polytechnica*, **53(6):** 906-912 (2013).

[13] Han Y., Wang J.J., Gu X.P., Feng L.F., Numerical Simulation on Micromixing of Viscous Fluids in a Stirred-Tank Reactor, *Chemical Engineering Science*, **74:** 9-17 (2012).

[14] Gu D., Ye M., Liu Z., Computational Fluid Dynamics Simulation of Solid-Liquid Suspension Characteristics in a Stirred Tank with Punched Circle Package Impellers, *International Journal of Chemical Reactor Engineering*, **18(9):** (2020).

[15] Zhang Q., Yang C., Mao Z.-S., Mu J., Large Eddy Simulation of Turbulent Flow and Mixing Time in a Gas–Liquid Stirred Tank, *Industrial and Engineering Chemistry Research*, **51(30):** 10124-10131 (2012).

[16] Sungkorn R., Derksen J.J., Khinast J.G., Modeling of Aerated Stirred Tanks with Shear-Thinning Power Law Liquids, *International Journal of Heat and fluid flow*, **36:** 153-166 (2012).

[17] Hu X., Ilgun A.D., Passalacqua A., Fox R.O., Bertola F., Milosevic M., Visscher F., CFD Simulations of Stirred-Tank Reactors for Gas-Liquid and Gas-Liquid-Solid Systems Using Openfoam®, *International Journal of Chemical Reactor Engineering*, **19(2):** 193-207 (2021).

[18] Gillissen J.J.J., Van den Akker H.E.A., Direct Numerical Simulation of the Turbulent Flow in a Baffled Tank Driven by a Rushton Turbine, *AIChE Journal*, **58(12):** 3878-3890 (2012).

[19] Gillissen J.J.J., Van den Akker H.E.A., Direct Numerical Simulation of a Turbulently Stirred Tank, 13th Eur. Conf. Mix. London, UK, (2009).

[20] Zhang G., Zhao H., Lv C., Liu Y., Zhang T.-A., "CFD Simulations of a Large-Scale Seed Precipitation Tank Stirred With Multiple Intermig Impellers", Light Metals 2015, John Wiley & Sons, Inc., 63-68 (2015).

[21] Kálal Z., Jahoda M., Fořt I., Modelling of the Bubble Size Distribution in an Aerated Stirred Tank: Theoretical and Numerical Comparison of Different Breakup Models, *Chemical and Process Engineering - Inzynieria Chemiczna i Procesowa*, **35(3):** 331-348 (2014).

[22] Gelves R., "CFD Simulation of Liquid-Liquid Dispersions in a Stirred Tank Bioreactor", *AIP Conference Proceedings, AIP Conference Proceedings* 1558, pp. 2229-2232, (2013).

[23] Basavarajappa M., Miskovic S., "Numerical Study of Single Phase Liquid Mixing in Stirred Tanks Fitted With Rushton Turbine and Standard Flotation Impeller", *ASME 2013 Int. Mech. Eng. Cong. Expo.*, San Diego, USA, (2013).

[24] Alopaeus V., Moilanen P., Laakkonen M., Analysis of Stirred Tanks with Two-Zone Models, *AIChE Journal*, **55(10):** 2545-2552 (2009).

[25] Javed K.H., Mahmud T., Zhu J.M., Numerical Simulation of Turbulent Batch Mixing in a Vessel Agitated by a Rushton Turbine, *Chemical Engineering and Processing: Process Intensification*, **45(2):** 99-112 (2006).

[26] Ranade V.V., "Computational Flow Modeling for Chemical Reactor Engineering", Academic Press, San Diego, Calif, (2002).

[27] Ranade V.V., Perrard M., Le Sauze N., Xuereb C., Bertrand J., Trailing Vortices of Rushton Turbine: Piv Measurements and Cfd Simulations with Snapshots Approach, *Chemical Engineering Research and Design*, **79(1):** 3-12 (2001).

[28] Chtourou W., Ammar M., Driss Z., Abid M.S., Effect of the Turbulence Models on Rushton Turbine Generated Flow in a Stirred Vessel, *Central European Journal of Engineering*, **1(4):** 380-389 (2011).

[29] Ammar M., Driss Z., Chtourou W., Abid M.S., Effects of Baffle Length on Turbulent Flows Generated in Stirred Vessels, *Central European Journal of Engineering*, **1(4):** 401-412 (2011).

[30] Heidari A., Cfd Simulation of Operational Parameters Effects on Mixing Quality of Two-Phase Gas-Liquid Flow in Agitated Vessel, *Modares Mechanical Engineering*, **18(8):** 9-18 (2018).

[31] Heidari A., Cfd Simulation of Impeller Shape Effect on Quality of Mixing in Two-Phase Gas–Liquid Agitated Vessel, *Chinese Journal of Chemical Engineering*, **28(11):** 2733-2745 (2020).

[32] Li D., Chen W., Effects of Impeller Types on Gas-Liquid Mixing and Oxygen Mass Transfer in Aerated Stirred Reactors, *Process Safety and Environmental Protection*, **158:** 360-373 (2022).

[33] Hinze J.O., "Turbulence", McGraw-Hill, New York ; London, 1975.

[34] Orszag S.A., Yakhot V., Flannery W.S., Boysan F., Choudhury D., Maruzewski J., Patel B., "Renormalization Group Modeling and Turbulence Simulations", *International Conference on Near-Wall Turbulent Flows*, Tempe, Arizona, USA (1993).

[35] Wu H., Patterson G.K., Laser-Doppler Measurements of Turbulent-Flow Parameters in a Stirred Mixer, *Chemical Engineering Science*, **44(10):** 2207-2221 (1989).